

Article

# Robust Sensorless Control of Interior Permanent Magnet Synchronous Motor Using Deadbeat Extended Electromotive Force Observer

Seung-Taik Kim, In-Sik Yoon, Sung-Chul Jung  and Jong-Sun Ko \*

Department of Electronic and Electrical Engineering, Dankook University, 152, Jukjeon-ro, Suji-gu, Yongin-si 16890, Korea

\* Correspondence: jsko@dankook.ac.kr

**Abstract:** This paper proposes a novel and robust method of sensorless speed control using a deadbeat observer for an interior permanent magnet synchronous motor (IPMSM). The proposed sensorless speed control method uses a deadbeat observer to estimate the extended electromotive force (EEMF) in a rotational coordinate system. The estimated EEMF is used in the IPMSM velocity estimation algorithm. The deadbeat EEMF observer (DEEMFO) shows greater robustness compared to the reconstructor, which estimates the EEMF by simply recalculating the voltage equation. Unlike a reconstructor, DEEMFO has a feedback component, so it can compensate for errors due to uncertainty in motor parameters and errors due to parameter fluctuations that may occur during use. By simulating and experimenting with speed, load torque, and parameter fluctuations, it is proved to be more robust and precise than the reconstructor. The simulation is performed with MATLAB/Simulink, and the experiments were carried out using a DSP TMS320F28335 and a motor-generator set (M-G Set). The simulation and experiment results show the reliability and precision of the proposed sensorless control method.

**Keywords:** interior permanent magnet synchronous motor; sensorless speed control; extended electromotive force; deadbeat observer



**Citation:** Kim, S.-T.; Yoon, I.-S.; Jung, S.-C.; Ko, J.-S. Robust Sensorless Control of Interior Permanent Magnet Synchronous Motor Using Deadbeat Extended Electromotive Force Observer. *Energies* **2022**, *15*, 7568. <https://doi.org/10.3390/en15207568>

Academic Editors: Kan Liu and Wei Hu

Received: 17 September 2022

Accepted: 9 October 2022

Published: 13 October 2022

**Publisher's Note:** MDPI stays neutral with regard to jurisdictional claims in published maps and institutional affiliations.



**Copyright:** © 2022 by the authors. Licensee MDPI, Basel, Switzerland. This article is an open access article distributed under the terms and conditions of the Creative Commons Attribution (CC BY) license (<https://creativecommons.org/licenses/by/4.0/>).

## 1. Introduction

IPMSM is widely applied in various driving fields that require high performance, power factor and efficiency, such as industrial facilities and electric vehicles. IPMSM has the advantages that it generates a high torque even with a small rotor size by generating magnetic torque as well as a reluctance torque due to its saliency [1,2]. To efficiently drive an AC motor such as the IPMSM, rotor speed and position information are required. A sensor such as an optical encoder or resolver is required to obtain this information. However, the installation and maintenance costs increase due to the use of the sensor. Furthermore, the problems with the sensor resolution and a bad installation environment cause issues due to errors and disturbances. Therefore, the research on sensorless control without those sensors has been conducted.

One of several methods of sensorless control is using electromotive force. It has a relatively simple structure and shows stable performance over a wide operating range [3–6]. However, when the AC motor is operating at a low speed, the generated back EMF is small, so it is difficult to properly estimate speed [7]. The electromotive force observer method includes a model reference adaptive system [8], extended Kalman filter [9], and sliding mode observer [10]. The second method is the high-frequency signal injection method. Its advantage is that speed and position can be estimated through the injected high frequency even at an extremely low operating speed [11–14]. However, there are losses and noise, additional components are needed for high frequency injection, and it is difficult to find and apply a suitable high frequency signal. Recently, in order to solve the limitations of

each method, various methods such as I/f control for low-speed region control [15], a nonlinear extended state observer [16], and a modified model reference adaptive system were being studied [17]. In particular, the sensorless method using electromotive force also has limitations in that it requires some approximation to be used in IPMSM. To solve this, a sensorless control method using an EEMF model that does not require approximation has been proposed in the stationary frame [18], and rotating frame [19].

The paper proposes a robust and innovative sensorless control method for IPMSM. The proposed method uses a deadbeat observer to estimate the EEMF in a rotating coordinate system. A deadbeat observer is easy to pole placement and can accurately estimate parameters using large gains [20]. The DEEMFO is more robust compared to the reconstructor, which estimates the EEMF by simply recalculating the voltage equation. Unlike a reconstructor, DEEMFO has a feedback component, so it can compensate for errors due to uncertainty in motor parameters and errors due to parameter fluctuations that may occur during use.

In this paper, the definition of EEMF and the reconstruction method for estimating it are explained first. The proposed DEEMFO, which solves the limitations of the reconstructor, is described in detail. After that, the simulation and experimental results are presented under conditions of no-load, speed change, load change, and parameter variation. The simulation and experiment results show the reliability and precision of the proposed sensorless control method.

## 2. The EEMF Estimation Algorithm

### 2.1. Mathematical Model of IPMSM

Figure 1 shows stationary and rotating reference frames. The  $\alpha$ - $\beta$  frame is a stationary frame fixed to the stator winding. The  $d$ - $q$  rotating reference frame is also known as a synchronous reference frame. In this coordinate system, the  $d$ -axis indicates the N pole direction of the permanent magnet. The  $q$ -axis indicates a direction that is 90 degrees in front of the  $d$ -axis by the electrical angle [21]. The IPMSM voltage equations for the  $d$ - $q$  rotation reference frame are expressed as (1) and (2):

$$\begin{bmatrix} v_d \\ v_q \end{bmatrix} = \begin{bmatrix} R_s + pL_d & -\omega L_q \\ \omega L_q & R_s + pL_d \end{bmatrix} \begin{bmatrix} i_d \\ i_q \end{bmatrix} + \begin{bmatrix} 0 \\ E_{ex} \end{bmatrix} \quad (1)$$

$$E_{ex} = \omega [(L_d - L_q)i_d + \lambda_{pm}] - (L_d - L_q)(pi_q) \quad (2)$$

where  $v_d, v_q$  are the values of stator voltage;  $i_d, i_q$  are the values of stator current;  $L_d, L_q$  are the values of stator inductance in the  $d$ - $q$  frame.  $R_s$  is the stator resistance,  $\omega$  is the rotor angular speed,  $\lambda_{pm}$  is the magnet flux linkage and  $p$  is the differential operator. The second term in (1) is called EEMF as (2) [19].

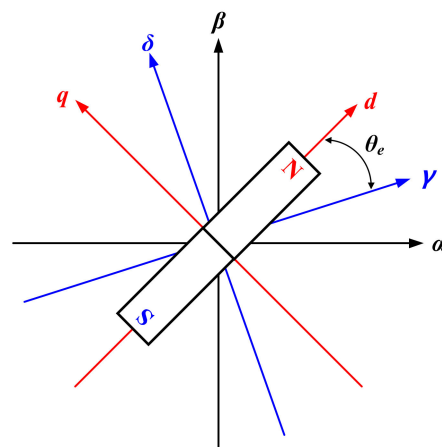


Figure 1. Reference frames for IPMSM Control.

In a sensorless system, speed and position are estimated. The estimated position is located on the  $\gamma$ - $\delta$  rotating frame, which differ from the actual  $d$ - $q$  frame by the position error  $\theta_e$ . Therefore, the voltage equations in the  $\gamma$ - $\delta$  reference frame can be expressed as (3) and (4):

$$\begin{bmatrix} v_\gamma \\ v_\delta \end{bmatrix} = \begin{bmatrix} R_s + pL_d & -\omega L_q \\ \omega L_q & R_s + pL_d \end{bmatrix} \begin{bmatrix} i_\gamma \\ i_\delta \end{bmatrix} + \begin{bmatrix} e_\gamma \\ e_\delta \end{bmatrix} \quad (3)$$

$$\begin{bmatrix} e_\gamma \\ e_\delta \end{bmatrix} = E_{ex} \begin{bmatrix} -\sin \theta_e \\ \cos \theta_e \end{bmatrix} + (\hat{\omega} - \omega)L_d \begin{bmatrix} -i_\delta \\ i_\gamma \end{bmatrix} \quad (4)$$

where  $v_\gamma, v_\delta$  are the values of the stator voltage;  $i_\gamma, i_\delta$  are the values of stator current;  $e_\gamma, e_\delta$  are the values of EEMF in the  $\gamma$ - $\delta$  frame;  $\hat{\omega}$  denotes the estimated value;  $R_s$  is the stator resistance;  $\omega$  is the rotor angular speed;  $\lambda_{pm}$  is the magnet flux linkage and  $p$  is the differential operator.

### 2.2. EEMF Estimation Using Reconstructor

Assuming that the error of the estimated velocity is small and can be considered 0, and the derivative of EEMF is zero, the EEMF can be estimated by the reconstructor using the state space Equations (5) and (6) [19]. This method can estimate the EEMF by simply reconstructing the voltage Equation (7):

$$p \begin{bmatrix} i_\gamma \\ e_\gamma \end{bmatrix} = \frac{1}{L_d} \begin{bmatrix} -R_s & -1 \\ 0 & 0 \end{bmatrix} \begin{bmatrix} i_\gamma \\ e_\gamma \end{bmatrix} + \frac{1}{L_d} \begin{bmatrix} 1 \\ 0 \end{bmatrix} (v_\gamma + \omega L_q i_\delta) \quad (5)$$

$$p \begin{bmatrix} i_\delta \\ e_\delta \end{bmatrix} = \frac{1}{L_d} \begin{bmatrix} -R_s & -1 \\ 0 & 0 \end{bmatrix} \begin{bmatrix} i_\delta \\ e_\delta \end{bmatrix} + \frac{1}{L_d} \begin{bmatrix} 1 \\ 0 \end{bmatrix} (v_\delta - \omega L_q i_\gamma) \quad (6)$$

$$\begin{bmatrix} \hat{e}_\gamma \\ \hat{e}_\delta \end{bmatrix} = \begin{bmatrix} v_\gamma + \hat{\omega} L_q i_\delta - (R_s + pL_d) i_\gamma \\ v_\delta - \hat{\omega} L_q i_\gamma - (R_s + pL_d) i_\delta \end{bmatrix} \quad (7)$$

where  $\hat{e}_\gamma, \hat{e}_\delta$  are the values of estimated EEMF and  $\hat{\omega}$  is estimated speed.

From Equation (7), the derivative term allows the reconstructor to estimate the EEMF even at low-speed operation if the current changes [18]. However, when the current changes rapidly due to changes in speed and load, the differential value of the current is very large and may cause system instability. Therefore, a low-pass filter is required. In addition, when applied to a digital system, if the current value is not measured because it does not match the sampling period when the current changes, the amount of change cannot be reflected in the calculation. Furthermore, in Equation (7) motor parameters are used that may be uncertain or changed during operation. If the parameter used for calculation in the reconstructor has a different value from the actual motor parameter, the calculated EEMF will have a different value from the actual value. If the calculated EEMF is used, the estimated speed value will of course have an error. However, it cannot compensate for parameter errors, so precise and robust control is not possible.

### 2.3. Proposed Deadbeat EEMF Observer

In this paper, we propose the novel EEMF estimation method using deadbeat observer. In the proposed DEEMFO, the EEMF estimation algorithm by the observer can solve the problem caused by the current differential term and compensate for the motor parameter variation by the feedback term. Through this feedback term, the difference between the actual value and the estimated value is multiplied by the observer gain, which has the effect of gradually reducing the error, even if the motor parameters are uncertain or there is variation. To ensure that the time required to calculate the EEMF is shorter than the entire system response time and to quickly compensate for errors, a deadbeat observer is desirable. As a result, DEEMFO is more robust to parameter fluctuations by reducing the error through the observer gain by receiving current feedback. In addition, the DEEMFO observer gain can be easily obtained and the system can quickly and stably use a large

observer gain. We reduced the size of the matrix for the calculation time, by dividing it along the  $\gamma$ - $\delta$  frame.

The observer formulas are expressed as Equations (8)–(13):

$$p \begin{bmatrix} \hat{i}_\gamma \\ \hat{e}_\gamma \end{bmatrix} = \frac{1}{L_d} \begin{bmatrix} -R_s & -1 \\ 0 & 0 \end{bmatrix} \begin{bmatrix} \hat{i}_\gamma \\ \hat{e}_\gamma \end{bmatrix} + \frac{1}{L_d} \begin{bmatrix} 1 \\ 0 \end{bmatrix} v_{\gamma 1} + \mathbf{e}k_\gamma \quad (8)$$

$$p \begin{bmatrix} \hat{i}_\delta \\ \hat{e}_\delta \end{bmatrix} = \frac{1}{L_d} \begin{bmatrix} -R_s & -1 \\ 0 & 0 \end{bmatrix} \begin{bmatrix} \hat{i}_\delta \\ \hat{e}_\delta \end{bmatrix} + \frac{1}{L_d} \begin{bmatrix} 1 \\ 0 \end{bmatrix} v_{\delta 1} + \mathbf{e}k_\delta \quad (9)$$

$$v_{\gamma 1} = v_\gamma + \hat{\omega} L_q i_\delta \quad (10)$$

$$v_{\delta 1} = v_\delta - \hat{\omega} L_q i_\gamma \quad (11)$$

$$\mathbf{e}k_\gamma = \begin{bmatrix} ek_{\gamma 1} \\ ek_{\gamma 2} \end{bmatrix} \left( i_\gamma - \begin{bmatrix} 1 & 0 \end{bmatrix} \begin{bmatrix} \hat{i}_\gamma \\ \hat{e}_\gamma \end{bmatrix} \right) \quad (12)$$

$$\mathbf{e}k_\delta = \begin{bmatrix} ek_{\delta 1} \\ ek_{\delta 2} \end{bmatrix} \left( i_\delta - \begin{bmatrix} 1 & 0 \end{bmatrix} \begin{bmatrix} \hat{i}_\delta \\ \hat{e}_\delta \end{bmatrix} \right) \quad (13)$$

where  $ek_{\gamma 1}$ ,  $ek_{\gamma 2}$ ,  $ek_{\delta 1}$ , and  $ek_{\delta 2}$  are observer gain.

The discrete observer can be expressed as Equations (14) and (15):

$$\begin{bmatrix} \hat{i}_\gamma[k+1] \\ \hat{e}_\gamma[k+1] \end{bmatrix} = \mathbf{A}_d \begin{bmatrix} \hat{i}_\gamma[k] \\ \hat{e}_\gamma[k] \end{bmatrix} + \mathbf{B}_d v_{\gamma 1} + \mathbf{E}K_\gamma (i_\gamma[k] - \hat{i}_\gamma[k]) \quad (14)$$

$$\begin{bmatrix} \hat{i}_\delta[k+1] \\ \hat{e}_\delta[k+1] \end{bmatrix} = \mathbf{A}_d \begin{bmatrix} \hat{i}_\delta[k] \\ \hat{e}_\delta[k] \end{bmatrix} + \mathbf{B}_d v_{\delta 1} + \mathbf{E}K_\delta (i_\delta[k] - \hat{i}_\delta[k]) \quad (15)$$

where  $\mathbf{A}_d$ ,  $\mathbf{B}_d$  are the system matrix and the input matrix.  $\mathbf{E}K_\gamma$ ,  $\mathbf{E}K_\delta$  are the observer gain matrices.

Since the rank of the observer ability matrix is 2, the observer is observable. This paper proposes and uses DEEMFO by applying the deadbeat observer as an observer to estimate the EEMF. Since the deadbeat observer places the desired pole arrangement at the origin (0, 0) of the unit concentric circle in the z-domain as shown in Figure 2, observer gain can be easily obtained and the system can quickly and stably use a large observer gain. The observer gain matrices  $\mathbf{E}K_\gamma$  and  $\mathbf{E}K_\delta$  can be calculated by the pole placement using Ackermann's formula [22]:

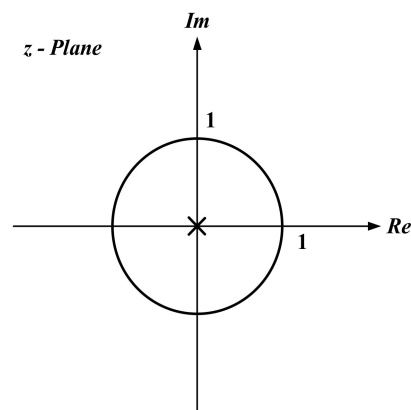


Figure 2. The z-plane for the deadbeat EEMF observer pole placement.

Figure 3 shows the block diagram of DEEMFO on the  $\gamma$ -axis. The  $\delta$ -axis also has the same configuration. In this system, the observer gain matrices  $\mathbf{E}K_\gamma$ ,  $\mathbf{E}K_\delta$  are equal to  $\mathbf{E}K_d$ , where  $\mathbf{C}_d$  is the output matrix. With voltage, current, stator inductance  $L_q$  and estimated speed as inputs, EEMF and current are estimated by DEEMFO.

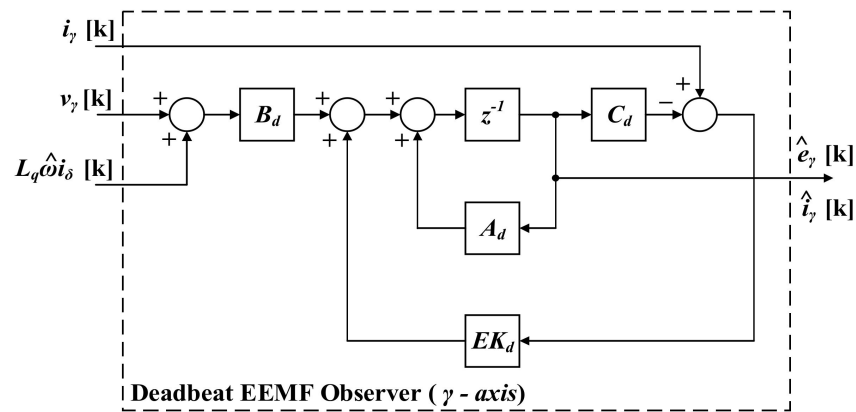


Figure 3. Block diagram of DEEMFO.

Since the difference between the real current  $i_\gamma, i_\delta$  and the estimated current  $\hat{i}_\gamma, \hat{i}_\delta$  is multiplied by the observer gain matrix  $EK_d$ , there is a feedback term to compensate for the parameter error and variation effects. After EEMF  $\hat{e}_\gamma, \hat{e}_\delta$  is estimated by the DEEMFO, the position error  $\hat{\theta}_e$  is estimated by Equation (16):

$$\hat{\theta}_e = \tan^{-1}\left(-\frac{\hat{e}_\gamma}{\hat{e}_\delta}\right) \tag{16}$$

Figure 4 shows the block diagram of the rotor speed and position estimation algorithm. The estimated position error  $\hat{\theta}_e$  is used to estimate the rotor speed. By compensating the estimated position error  $\hat{\theta}_e$  to be 0 using the PI compensator, the rotor speed is obtained and the rotor position is estimated by its integration.

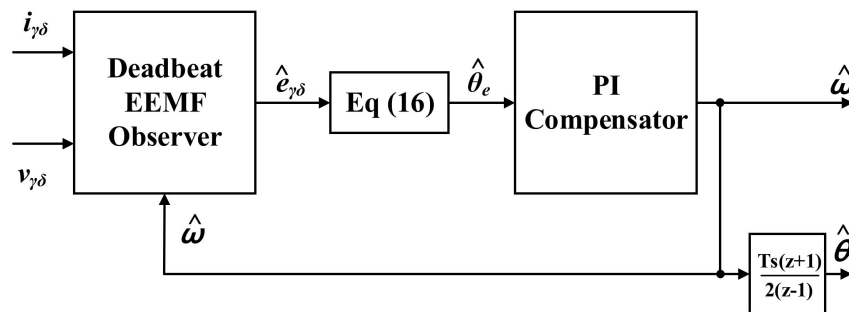


Figure 4. Block diagram of the rotor speed and position estimation algorithm.

Figure 5 represents the proposed overall system block diagram including maximum torque per ampere (MTPA) control for efficient IPMSM control and pulse width modulation (PWM) control along with the proposed speed estimation algorithm. When the speed command  $\omega^*$  is an input of the speed controller, a torque command  $T_{com}$  is output to drive the IPMSM at the appropriate speed. The torque command  $T_{com}$  is used as an input of the MTPA and outputs the command current  $i_{dq}^*$ . The voltage commands  $v_{dq}^*$  obtained by the current controller (PI controller) are converted to three-phase and input into the pulse width modulation (PWM) inverter. The real stator current  $i_{dq}$  and the voltage commands  $v_{dq}^*$  are used for the DEEMFO input. By applying the speed and position estimation algorithm, the system of Figure 5 performs the sensorless control of the IPMSM.

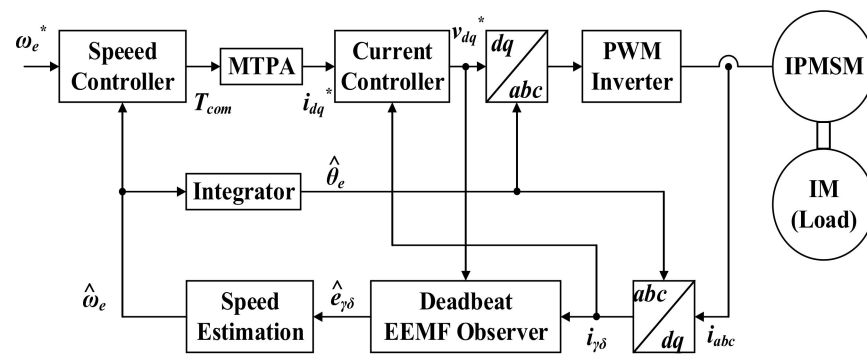


Figure 5. Block diagram of the sensorless speed control system using the proposed deadbeat EEMF Observer.

### 3. Simulation

#### 3.1. Set-Up

The simulations are performed by MATLAB/Simulink. In the simulation part, the results are analyzed using DEEMFO and compared with the reconstructor. The IPMSM parameters applied to the simulation and experiment are shown in Table 1.

Table 1. IPMSM Parameters.

Parameter	Value	Unit
Rated power	4.0	kW
Rated speed	3500	r/min
Rated torque	12	Nm
Rated voltage	380	V
Rated Current	10	A
Stator resistance ( $R_s$ )	0.332	$\Omega$
Inductance d-axis ( $L_d$ )	9.91	mH
Inductance q-axis ( $L_q$ )	10.93	mH
Flux linkage	0.118	Wb
Pole pairs	5	-

Figure 6 shows the configuration of the proposed IPMSM sensorless control with the use of the DEEMFO simulator. The simulator includes DEEMFO, speed estimation algorithm, speed controller, MTPA operation, current controller, and space vector PWM (SVPWM) inverter. It was designed in the same way as shown in Figure 5. The DEEMFO sampling frequency is 5 kHz, the current controller is 5 kHz, and the speed controller is 0.5 kHz. The switching frequency of the SVPWM inverter has been set to 5 kHz.

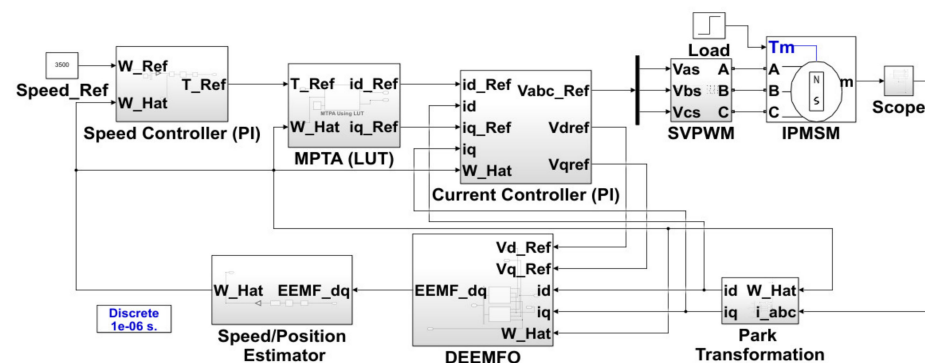


Figure 6. MATLAB/Simulink simulator for IPMSM sensorless control.

Robust and precise sensorless speed control requires accurate rotor speed and position estimation even if the speed or load torque increases or decreases rapidly or parameters

are uncertain or changed. To verify this, the simulation was compared and verified under four conditions. First, the control results were compared using the reconstructor and the proposed DEEMFO under no-load conditions; second, when there is a speed command change from 3000 rpm to 3500 rpm; and third, when the load torque increases from 0 Nm to 6 Nm, which is half of the rated torque. As the most important condition, the results were compared by changing the stator resistance  $R_s$  and the stator inductance  $L_d, L_q$  by 30%, assuming there was a parameter variation or if there are errors in the parameter values in the datasheet.

3.2. Simulation Result

Figure 7 shows the simulation results under no-load conditions using the reconstructor and the proposed DEEMFO. It shows the actual rotor speed  $\omega_r$  estimated speed  $\hat{\omega}_r$ , reference speed  $\omega_r^*$ , stator current  $\hat{i}_\gamma, \hat{i}_\delta$ , and the error as the difference between the actual speed/position and the estimated speed/position.

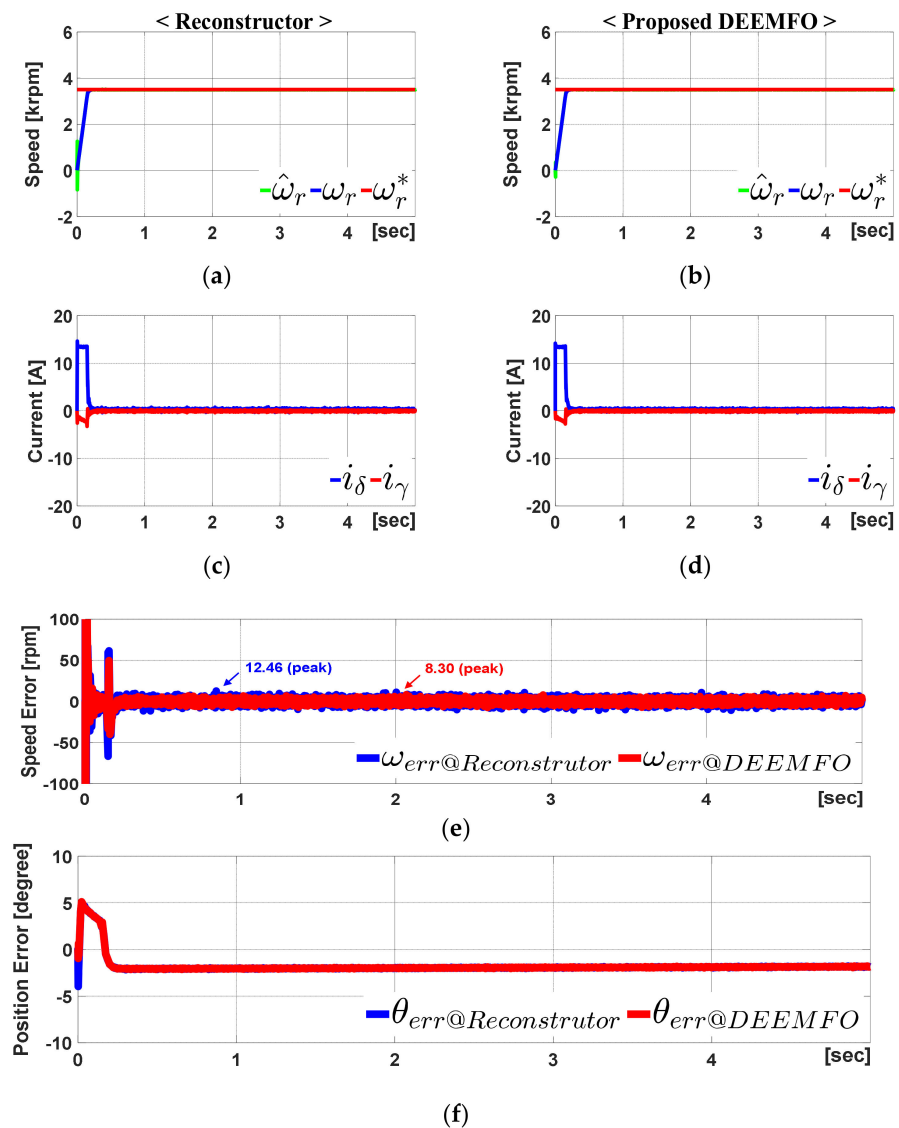
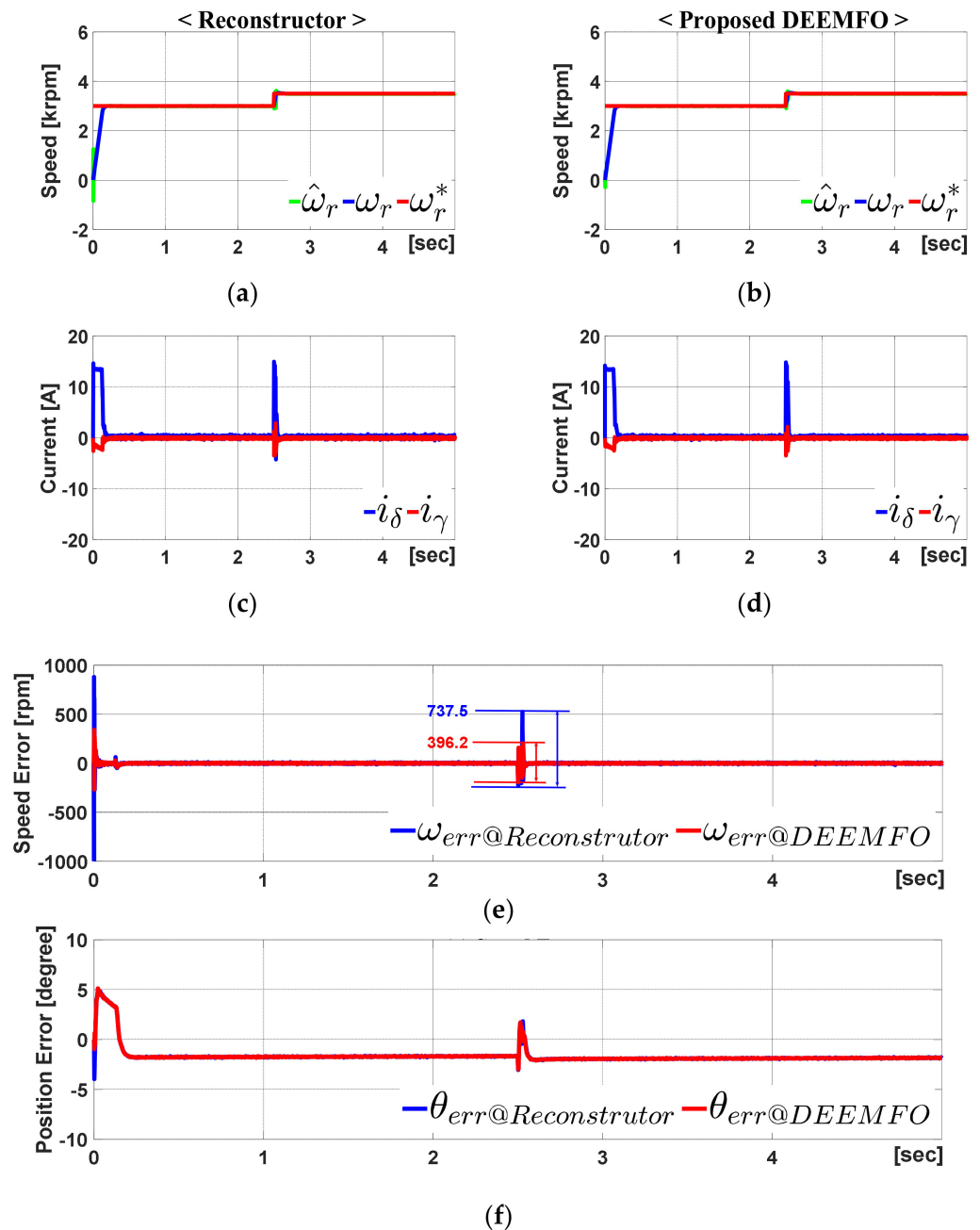


Figure 7. Simulation results under no load condition. (a) reference, real, and estimated speed with reconstructor; (b) reference, real, and estimated speed with DEEMFO; (c)  $\gamma - \delta$  axis currents with reconstructor; (d)  $\gamma - \delta$  axis currents with DEEMFO; (e) comparison of speed errors in reconstructor and DEEMFO; (f) comparison of position errors in reconstructor and DEEMFO.

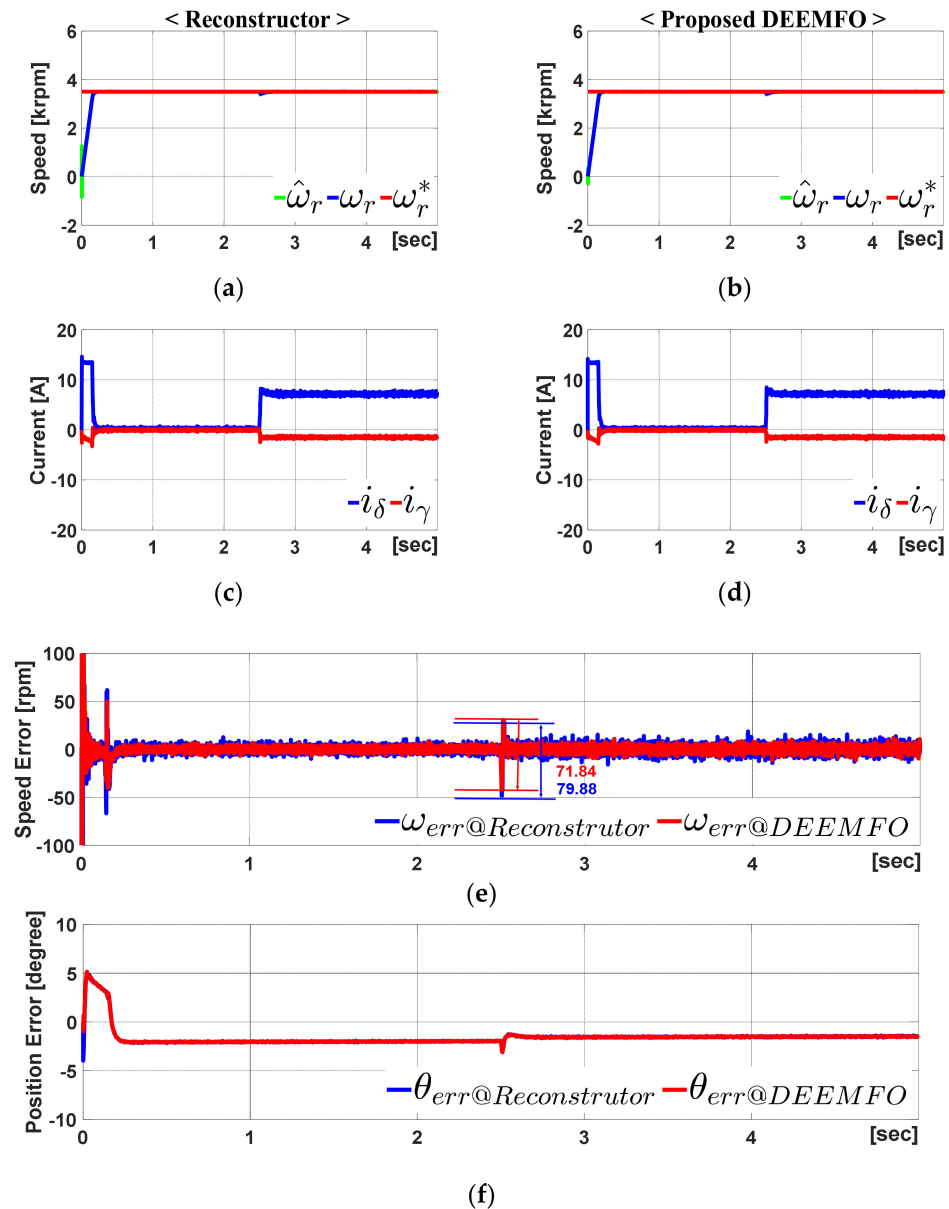
When using the reconstructor, it peaks at around 12.46 rpm at a steady state, and when applying the DEEMFO, it shows a peak value of about 8.30 rpm and the speed error of around 4 rpm is reduced. This means an error improvement of approximately 33.4%.

Figure 8 summarizes the results under the condition that the speed command increased from 3000 rpm to 3500 rpm. When the speed command increases at 2.5 s, a speed error  $\omega_{err}$  occurs. At this time, the speed error when using the reconstructor is 737.5 rpm, and the speed error when using the proposed DEEMFO is 396.2 rpm. This means an error improvement of approximately 46.3%.



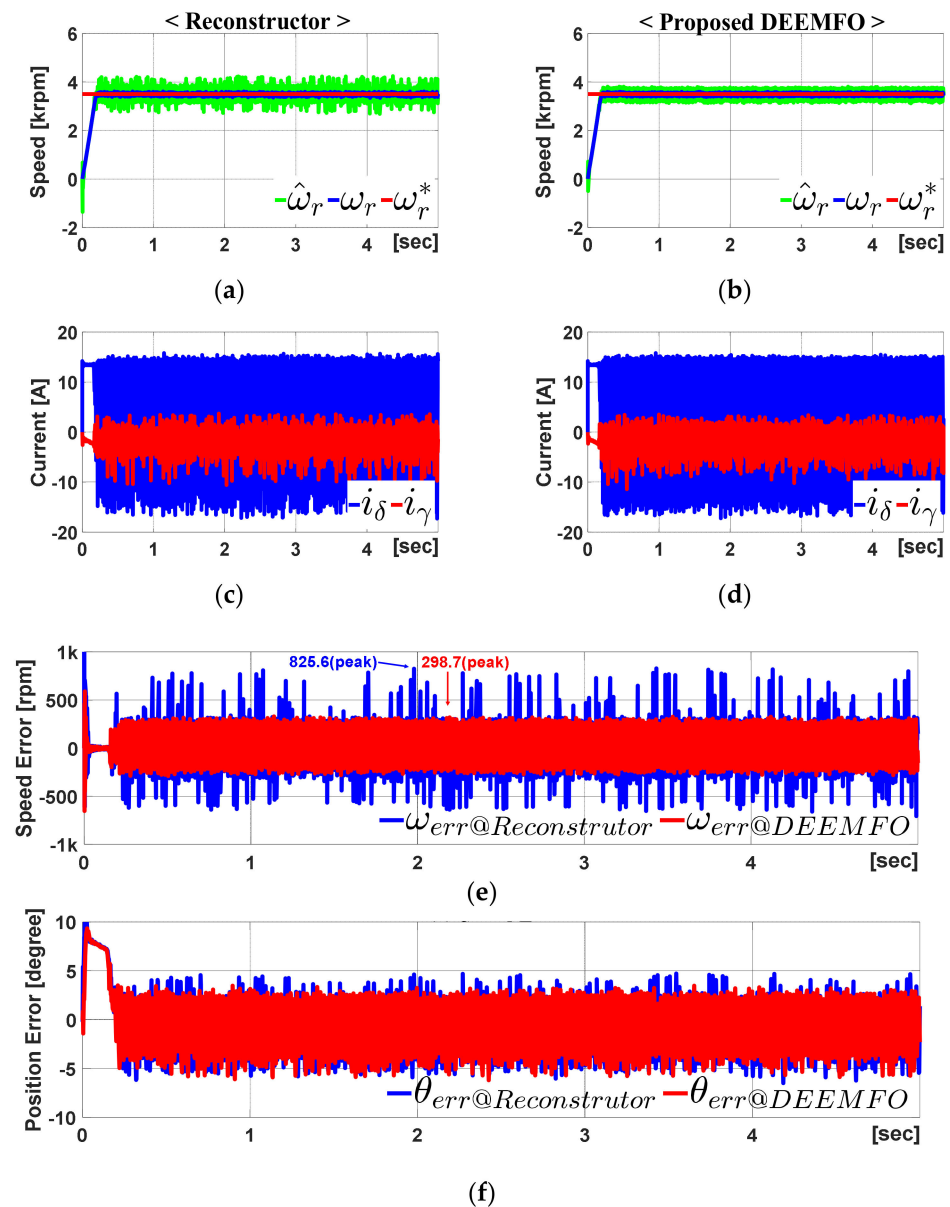
**Figure 8.** Simulation results under the condition that the speed reference increased from 3000 rpm to 3500 rpm. (a) reference, real, and estimated speed with reconstructor; (b) reference, real, and estimated speed with DEEMFO; (c)  $\gamma - \delta$  axis currents with reconstructor; (d)  $\gamma - \delta$  axis currents with DEEMFO; (e) comparison of speed errors in reconstructor and DEEMFO; (f) comparison of position errors in reconstructor and DEEMFO.

Figure 9 summarizes the simulation results provided for the load torque increased from 0 Nm to 6 Nm. It exhibits excellent control performance due to its high and accurate speed. Figure 9 shows also the speed and position error. In the reconstruction method, a speed error  $\omega_{err}$  is 79.88 rpm. In contrast, meanwhile, in DEEMFO there is a speed error  $\omega_{err}$  of about 71.84 rpm. This means an error improvement of about 10.1%.



**Figure 9.** Simulation results under the condition of increasing the load torque from 0 Nm to 6 Nm. (a) reference, real, and estimated speed with reconstructor; (b) reference, real, and estimated speed with DEEMFO; (c)  $\gamma - \delta$  axis currents with reconstructor; (d)  $\gamma - \delta$  axis currents with DEEMFO; (e) comparison of speed errors in reconstructor and DEEMFO; (f) comparison of position errors in reconstructor and DEEMFO.

Figure 10 represents a summary of the simulation results, provided that the IPMSM parameters changed by 30%. The speed error  $\omega_{err}$  of the reconstructor is greater than the proposed DEEMFO. The detail value is shown in Figure 10. The speed error  $\omega_{err}$  is approximately 825.6 rpm when the reconstructor is used. However, when applying DEEMFO, the speed error  $\omega_{err}$  is around 298.7 rpm. This means an error improvement of about 63.8%.



**Figure 10.** Simulation results under the condition that the parameter changed by 30%. (a) reference, real, and estimated speed with reconstructor; (b) reference, real, and estimated speed with DEEMFO; (c)  $\gamma - \delta$  axis currents with reconstructor; (d)  $\gamma - \delta$  axis currents with DEEMFO; (e) comparison of speed errors in reconstructor and DEEMFO; (f) comparison of position errors in reconstructor and DEEMFO.

The control performance was compared by simulating it according to several parameter variations. Table 2 shows whether the sensorless speed control of the reconstructor and DEEMFO is possible when the motor parameter varies from 0.72 pu to a maximum of 1.79 pu. The reconstructor becomes a stable sensorless control only when the electrical parameters ( $R_s$ ,  $L_d$ ,  $L_q$ ) of the actual motor change from 0.94 pu to 1.54 pu. However, when the proposed DEEMFO is applied, stable sensorless control is possible, even if the parameters range from 0.73 pu to 1.79 pu. If the actual motor parameter and the parameter used to estimate the EEMF are different, it can be analyzed that the error is large because the difference cannot be compensated for, because there is no internal feedback. However, if DEEMFO is applied, relatively quick and robust control can be achieved.

**Table 2.** Speed control result according to parameter change.

Parameter Variation	Reconstructor	DEEMFO
$(R_s, L_d, L_q) \times 0.72$	X	X
$(R_s, L_d, L_q) \times 0.73$	X	O
⋮	X	O
$(R_s, L_d, L_q) \times 0.94$	O	O
⋮	O	O
$(R_s, L_d, L_q) \times 1.00$	O	O
⋮	O	O
$(R_s, L_d, L_q) \times 1.54$	O	O
$(R_s, L_d, L_q) \times 1.55$	O	O
⋮	X	O
$(R_s, L_d, L_q) \times 1.78$	X	O
$(R_s, L_d, L_q) \times 1.79$	X	X
$(R_s, L_d, L_q) \times 0.72$	X	X
$(R_s, L_d, L_q) \times 0.73$	X	O
⋮	X	O

**4. Experiment**

*4.1. Set-Up*

Figure 11 shows the M-G set wiring diagram for the experiment. The DSP TMS320F38225 controller, M-G Set, and measuring equipment are connected. Three-phase power is applied to the IPMSM through the power module. The encoder, an IPMSM position sensor, is connected to the controller to measure the actual position, but this position information is not used for actual control as it is sensorless control. The 5.5 kW induction motor (IM) for applying load torque operates via a commercial driver. The control system consists of the controller and easyDSP to output parameters such as position, speed, voltage command, and current command from the IPMSM and a torque sensor/display for checking speed and torque. A 12-bit oscilloscope was connected to obtain a waveform as a result of the experiment. The experimental devices are shown in Figures 12 and 13.

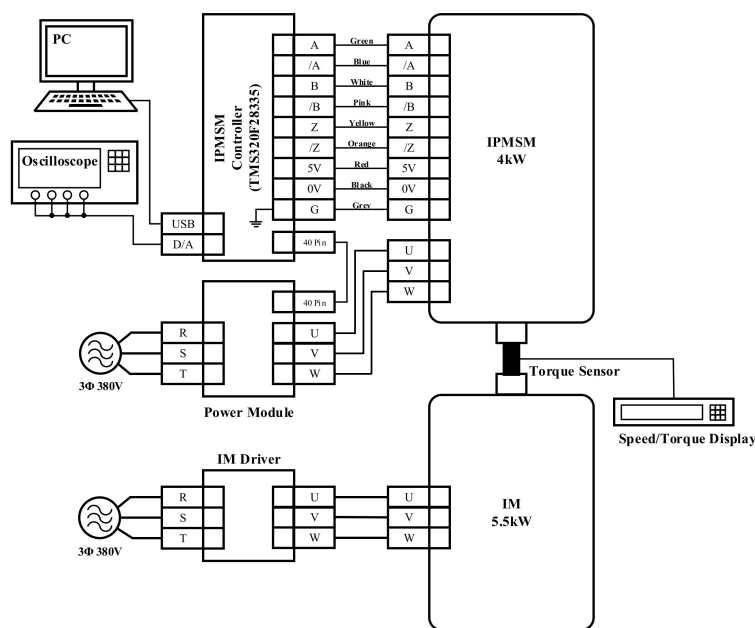


**Figure 11.** M-G set wiring diagram for experiment.

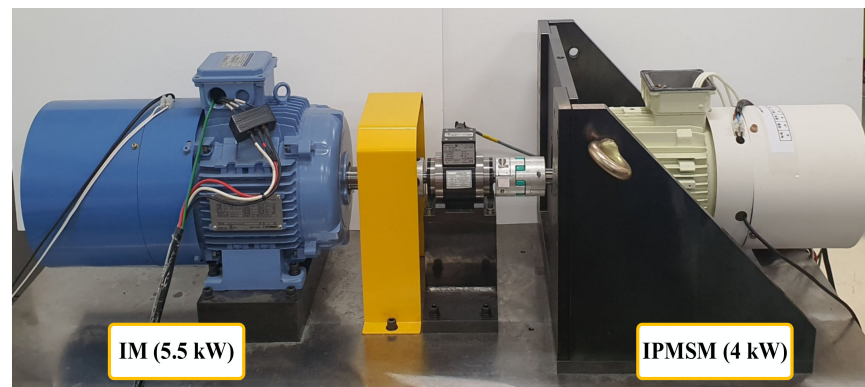


Figure 12. M-G set for the experiment.

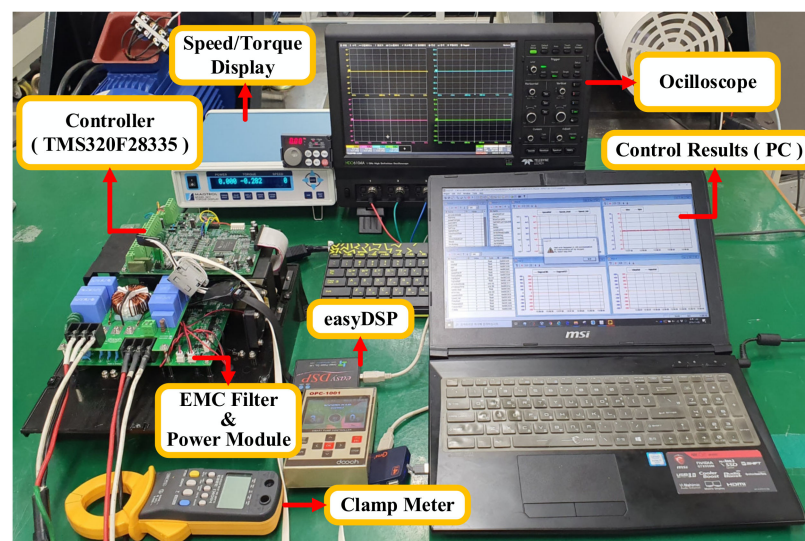


Figure 13. Device configuration for experiments.

#### 4.2. Experiment Result

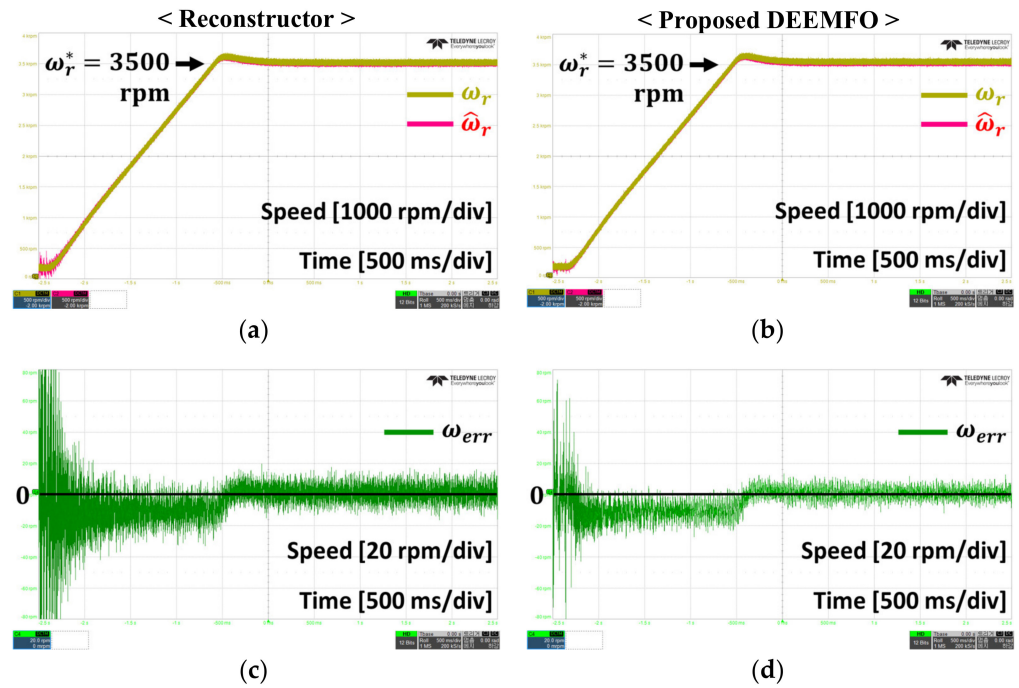
The experiment was conducted under four conditions as in the simulation. Figure 14 shows the speed obtained in the IPMSM sensorless speed control experiment under no load conditions. It can be seen that the speed error  $\omega_{err}$  is smaller in the results when using DEEMFO than in the reconstruction method. The experimental results were analyzed to be the same as the simulation results.

Figure 15 shows the results when changing the speed from 3000 rpm to 3500 rpm. The reconstructor has a speed error  $\omega_{err}$  with a peak-to-peak value of 50.4 rpm. However, using DEEMFO, the speed error  $\omega_{err}$  reaches a peak-to-peak value of 40.3 rpm. It shows an error improvement of about 20.0%.

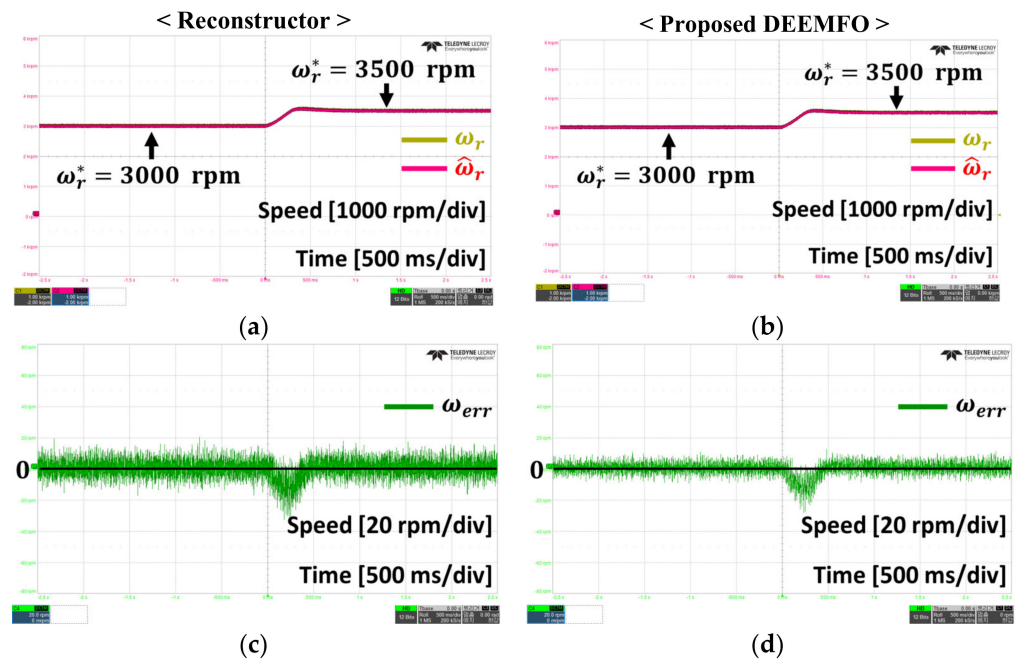
Figure 16 represents the results when the load torques were changed from 0 Nm to 6 Nm. In the experiment, the load torque does not increase rapidly due to the limitation of the induction motor applying the load torque, so the speed error is small compared to the simulation. However, even as the load torque increases, the speed error  $\omega_{err}$  is smaller when the DEEMFO is used compared to the conventional system. The speed error  $\omega_{err}$  was measured in the control method by the conventional method, reaching a peak-to-peak value of 53.7 rpm. However, the experiment results obtained via the proposed DEEMFO showed the peak-to-peak error equal to 41.6 rpm. It shows an error improvement of about 22.5%.

Figure 17 shows the results of the experiment carried out with the assumption that the electrical parameter of IPMSM increased by 30%. Since it is difficult to directly change the parameters of the IPMSM, we experimented by applying a factor of 1.3 to the nominal parameter. In the case of IPMSM electrical parameters' variation, the peak-to-peak error

of 34.6 rpm was measured in the control method using the reconstructor. However, in the control method using the proposed DEEMFO, the peak-to-peak error equals to 21.6 rpm. It shows an error improvement of about 37.6%.



**Figure 14.** Summary of the experiment results under no load condition. (a) reference, real, and estimated speed with reconstructor; (b) reference, real, and estimated speed with DEEMFO; (c) speed error in reconstructor; (d) speed error in DEEMFO.



**Figure 15.** Summary of the experiment results on the condition of increasing the speed reference from 3000 rpm to 3500 rpm. (a) reference, real, and estimated speed with reconstructor; (b) reference, real, and estimated speed with DEEMFO; (c) speed error in reconstructor; (d) speed error in DEEMFO.

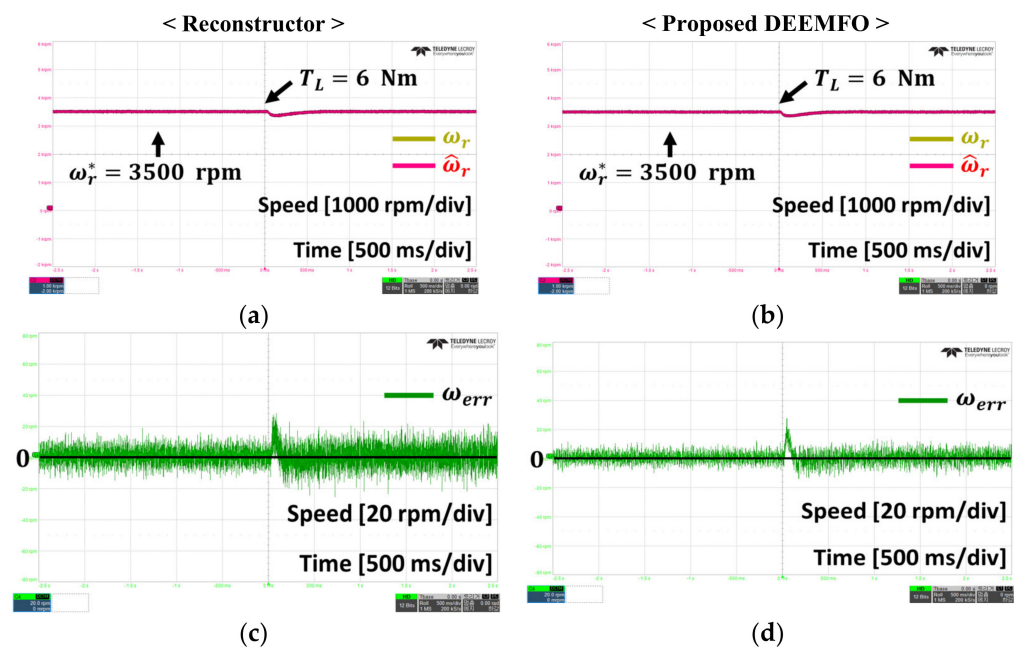


**Figure 16.** Summary of the experiment results under the condition of increasing the load torque from 0 Nm to 6 Nm. (a) reference, real, and estimated speed with reconstructor; (b) reference, real, and estimated speed with DEEMFO; (c) speed error in reconstructor; (d) speed error in DEEMFO.

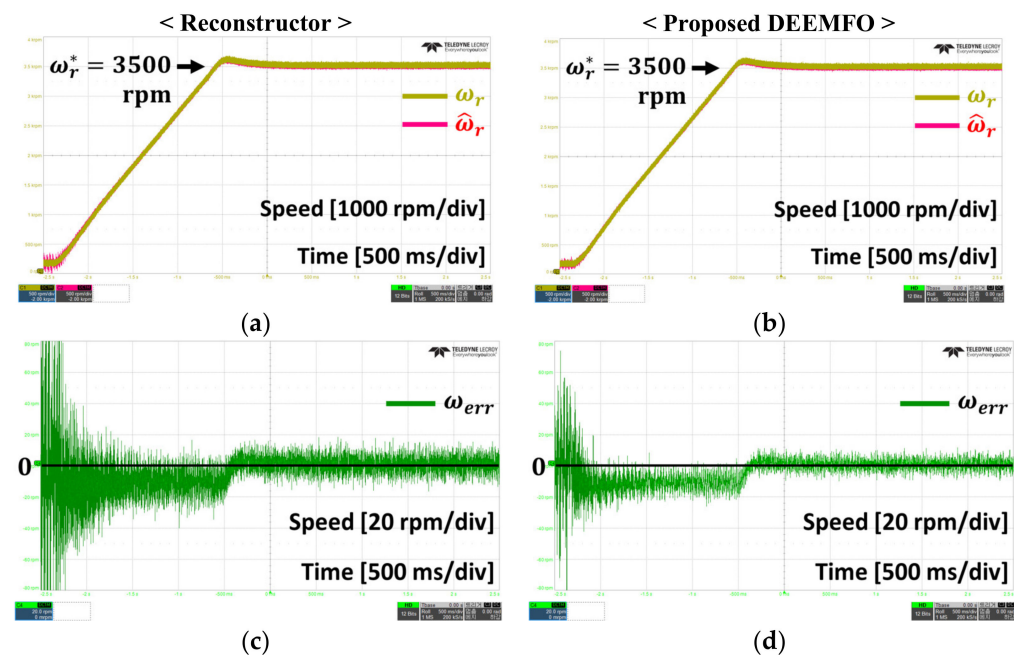


**Figure 17.** Summary of the experiment results provided for the parameters of IPMSM changed by 30%. (a) reference, real, and estimated speed with reconstructor; (b) reference, real, and estimated speed with DEEMFO; (c) speed error in reconstructor; (d) speed error in DEEMFO.

Through experiments under various conditions, it was experimentally verified that the proposed control method using DEEMFO is more accurate than the control method using the conventional method. By more accurately estimating the actual speed, it is possible to obtain control performance with more stable and robust dynamic characteristics even in terms of speed, load torque fluctuation, and parameters' variation.

## 5. Conclusions

In this paper, by estimating the EEMF using the deadbeat observer for sensorless speed control of IPMSM, it was shown that the speed control is robust and precise in various situations. DEEMFO was proposed to overcome the problem of the current differential term of the reconstructor and the limitation of being vulnerable to parameter fluctuations because the EEMF estimation relies only on simple formulas. DEEMFO can reduce the error between the actual value and the estimated value by compensating through the feedback term. Therefore, the sensorless speed control using the proposed DEEMFO has the advantage of being more precise, robust, and easy to apply because the observer gain can be easily obtained.

Through simulations and experimental results, the proposed DEEMFO shows a better speed control performance than the reconstructor under four conditions. As a result of analyzing the speed error of the reconstructor and DEEMFO, the speed error was improved by at least 10%. To be more precise, in the no-load condition, the error improvement effect of about 33.4% and about 20% compared to the reconstructor was proven in simulation and experiment, respectively. Error improvements of about 46.3% and about 20.0% in the simulation and experiment under the speed fluctuation condition and about 10.1% and 22.5% under the load fluctuation condition were proven, respectively. In particular, in the presence of parameter variations and errors, DEEMFO improves error by about 63.8% in simulation and about 37.6% in experiment.

Research will be conducted to improve operation in the low-speed range and to apply it to IPMSM of various capacities so that it can be used universally and stably. The IPMSM sensorless speed control method using DEEMFO is expected to be applicable to electric vehicles that have a lot of load fluctuations and motor parameters that can vary depending on weather and usage environment. It can also be used in pumps that are located in wet and hot basements and have a high risk of sensor failure.

**Author Contributions:** Conceptualization, S.-T.K. and I.-S.Y.; Formal analysis, S.-T.K. and I.-S.Y.; Investigation, S.-T.K.; Project administration, J.-S.K.; Software, S.-T.K.; Supervision, S.-C.J. and J.-S.K.; Validation, S.-C.J. and J.-S.K.; Writing—original draft, S.-T.K. All authors have read and agreed to the published version of the manuscript.

**Funding:** The work was supported in part by the Department of Electronics and Electrical Engineering, through the Research-Focused Department Promotion Project as a part of the University Innovation Support Program for Dankook University in 2021, and in part by a Korea Institute for Advancement of Technology grant funded by the MOTIE “The Competency Development Program for Industry specialist” (Foster R&D specialist of parts for eco-friendly vehicle (xEV), under Grant P0017120).

**Conflicts of Interest:** The authors declare no conflict of interest.

## References

1. Zhu, S.; Hu, Y.; Liu, C.; Jiang, B. Shaping of the Air Gap in a V-Typed IPMSM for Compressed-Air System Applications. *IEEE Trans. Magn.* **2021**, *57*, 8103705. [[CrossRef](#)]
2. Yang, Y.; Sandra, M.C.; Rong, Y.; Berker, B.; Anand, S.; Hossein, D.; Ali, E. Design and Comparison of Interior Permanent Magnet Motor Topologies for Traction Applications. *IEEE Trans. Transp. Electrification*. **2017**, *3*, 86–97. [[CrossRef](#)]
3. Lin, F.-J.; Hung, Y.-C.; Chen, J.-M.; Yeh, C.-M. Sensorless IPMSM drive system using saliency back-EMF-based intelligent torque observer with MTPA control. *IEEE Trans. Ind. Inform.* **2014**, *10*, 1226–1241.
4. Wang, G.; Yang, R.; Xu, D. DSP-Based control of sensorless IPMSM drives for wide-speed-range operation. *IEEE Trans. Ind. Electron.* **2012**, *60*, 720–727. [[CrossRef](#)]
5. Genduso, F.; Miceli, R.; Rando, C.; Galluzzo, G.R. Back EMF Sensorless-Control Algorithm for High-Dynamic Performance PMSM. *IEEE Trans. Ind. Electron.* **2010**, *57*, 2092–2100. [[CrossRef](#)]
6. Mobarakeh, B.N.; Tabar, F.M.; Sargos, F.M. Mechanical sensorless control of PMSM with online estimation of stator resistance. *IEEE Trans. Ind. Appl.* **2004**, *40*, 457–471. [[CrossRef](#)]
7. Sun, J.; Zhao, J.; Tian, L.; Song, Y.; Liu, Y. Bandwidth and Audible Noise Improvement of Sensorless IPMSM Drives based on Amplitude Modulation Multi-random Frequency Injection. *IEEE Trans. Power Electron.* **2022**, *37*, 14126–14140. [[CrossRef](#)]

8. Pal, A.; Das, S.; Chattopadhyay, A.K. An Improved Rotor Flux Space Vector Based MRAS for Field-Oriented Control of Induction Motor Drives. *IEEE Trans. Power Electron.* **2018**, *33*, 5131–5141. [[CrossRef](#)]
9. Yin, Z.; Li, G.; Zhang, Y.; Liu, J.; Sun, X.; Zhong, Y. A Speed and Flux Observer of Induction Motor Based on Extended Kalman Filter and Markov Chain. *IEEE Trans. Power Electron.* **2017**, *32*, 7096–7117. [[CrossRef](#)]
10. Wang, G.; Li, Z.; Zhang, G.; Yu, Y.; Xu, D. Quadrature PLL-Based High-Order Sliding-Mode Observer for IPMSM Sensorless Control with Online MTPA Control Strategy. *IEEE Trans. Energy Convers.* **2013**, *28*, 214–224. [[CrossRef](#)]
11. Zhang, G.; Wang, G.; Yuan, B.; Liu, R.; Xu, D. Active Disturbance Rejection Control Strategy for Signal Injection-Based Sensorless IPMSM Drives. *IEEE Trans. Transp. Electrif.* **2018**, *4*, 330–339. [[CrossRef](#)]
12. Tang, Q.; Shen, A.; Luo, X.; Xu, J. IPMSM sensorless control by injecting bidirectional rotating HF carrier signals. *IEEE Trans. Power Electron.* **2018**, *33*, 10698–10707. [[CrossRef](#)]
13. Kim, S.-Y.; Ha, I.J. A new observer design method for HF signal injection sensorless control of IPMSMs. *IEEE Trans. Ind. Electron.* **2008**, *55*, 2525–2529.
14. Bolognani, S.; Oboe, R.; Zigliotto, M. Sensorless full-digital PMSM drive with EKF estimation of speed and rotor position. *IEEE Trans. Ind. Electron.* **1999**, *46*, 184–191. [[CrossRef](#)]
15. Song, Z.; Yao, W.; Lee, K.; Li, W. An Efficient and Robust I-f Control of Sensorless IPMSM With Large Startup Torque Based on Current Vector Angle Controller. *IEEE Trans. Power Electron.* **2022**, *37*, 15308–15321. [[CrossRef](#)]
16. Zhang, Y.; Yin, Z.; Bai, C.; Wang, G.; Liu, J. A Rotor Position and Speed Estimation Method Using an Improved Linear Extended State Observer for IPMSM Sensorless Drives. *IEEE Trans. Power Electron.* **2021**, *36*, 14062–14073. [[CrossRef](#)]
17. Sun, X.; Zhang, Y.; Tian, X.; Cao, J.; Zhu, J. Speed Sensorless Control for IPMSMs Using a Modified MRAS With Gray Wolf Optimization Algorithm. *IEEE Trans. Electrif.* **2022**, *8*, 1326–1337. [[CrossRef](#)]
18. Chen, Z.; Tomita, M.; Doki, S.; Okuma, S. An extended electromotive force model for sensorless control of interior permanent-magnet synchronous motors. *IEEE Trans. Ind. Electron.* **2003**, *50*, 288–295. [[CrossRef](#)]
19. Morimoto, S.; Kawamoto, K.; Sanada, M.; Takeda, Y. Sensorless control strategy for salient-pole PMSM based on extended EMF in rotating reference frame. *IEEE Trans. Ind. Appl.* **2002**, *38*, 1054–1061. [[CrossRef](#)]
20. Ko, J.S.; Lee, J.H.; Chung, S.K.; Youn, M.J. A robust digital position control of brushless DC motor with deadbeat load torque observer. *IEEE Tran. Ind. Elec.* **1993**, *40*, 512–520. [[CrossRef](#)]
21. Bose, B.K. *Modern Power Electronics and AC Drives*; Prentice-Hall Inc.: Upper Saddle River, NJ, USA, 2002.
22. Astrom, K.J.; Wittenmark, B. *Computer-Controlled Systems: Theory and Design*, 3rd ed.; Prentice Hall: Hoboken, NJ, USA, 1996.